Australian Government

Department of Defence

Defence Science and Technology Group

# Evaluation of a Distributed Fibre Optic Strain Sensing System for Full- Scale Fatigue Testing

*Claire Davis, Meg Knowles and Geoff Swanton*

**Aerospace Division**
**Defence Science and Technology Group**

**DST-Group-TR-3452**

**ABSTRACT**

This report details an experimental comparison between the performance of conventional electrical resistance foil strain gauges and a commercially available fibre optic distributed strain measurement system based on Rayleigh scattering. Results are presented which compare strain response, spatial resolution and noise levels between the two systems, firstly on coupon specimens containing fatigue-induced cracks and secondly on a full-scale fatigue test article consisting of a centre barrel of an ex-service F/A-18 under simulated operational loading spectrum.

**RELEASE LIMITATION**

*Approved for public release.*

*Produced by*

*Aerospace Division*
*506 Lorimer Street*
*Fishermans Bend, VIC, 3207*

*Telephone: 1300 333 362*


*March 2018*
*AR-017-091*

# Evaluation of a Distributed Fibre Optic Strain Sensing System for Full-Scale Fatigue Testing

## Executive Summary

Current industry practice for the measurement of strain is the electrical resistance foil strain gauge. These sensors are time consuming to install and require three shielded wires per sensor, which can add considerable weight and complexity to the structure under test when high-density strain surveys are required. Electrical gauges are also prone to fatigue and require frequent calibration when installed on operational aircraft. Distributed fibre optic strain measurement systems present the opportunity to significantly reduce installation costs and complexity as well as addressing some of the durability and performance issues associated with electrical gauges.

This report details an experimental comparison between the performance of conventional electrical resistance foil strain gauges and a commercially available fibre optic distributed strain measurement system based on Rayleigh scattering. The results presented compare strain response, spatial resolution and noise levels between the two systems, firstly on coupon specimens containing fatigue-induced cracks and secondly on a full-scale fatigue test article consisting of a centre barrel of an ex-service F/A-18 subject to simulated operational spectrum loading.

In most areas the optical strain data compares well with measurements made using foil strain gauges however, there are some limitations to the system particularly when measuring strains in regions of high strain gradient. Despite these limitations, in many cases there is potential for Rayleigh scattering to provide detailed strain measurements at a substantially reduced cost per sensing point compared to conventional electrical resistance foil strain gauges.

*This page is intentionally blank.*

# Authors


## Claire Davis
Aerospace Division


*Claire Davis graduated with a Bachelor of Science (Honours) in Mathematics and Physics from Trinity College Dublin in 1991 and a Master of Science in Optoelectronics from the Queens University in Belfast in 1992. She completed a PhD in 1999 in fibre optic sensing at Swinburne University in Melbourne. From 1999-2002 she worked as a post-doctoral fellow at the National Centre for Sensor Research in Dublin prior to joining DST in 2002 as a research scientist. She is currently a senior research scientist working on the development of fibre optic sensors for structural health monitoring of Defence platforms.*

---


## Meg Knowles
Aerospace Division


*Meg Knowles is an undergraduate student at Swinburne University of Technology studying a double Bachelor of Engineering (Robotics/Mechatronics) and Science (Computer Science/Software Engineering). She is currently on a 12 month Industrial Experience Placement at the Defence Science and Technology Group.*

---


## Geoff Swanton
Aerospace Division


*Geoff Swanton graduated in 1992 from the Royal Melbourne Institute of Technology with an honours degree in Aeronautical Engineering. The following year he commenced work at the then Aeronautical Research Laboratory supporting various F-111 Structural Integrity projects. His Durability and Damage Tolerance (DADTA) work culminated in a 20-month posting to Lockheed Martin (Fort Worth, Texas) from 1998 to 2000 where he performed DADTA analyses and crack growth software development. From mid-2001 to mid-2003, Geoff was Staff Officer (Science) – Strike Reconnaissance at RAAF Base Amberley, where he was engaged in technical liaison activities in support of F-111 engineering and operations. From mid-2006 to mid-2007 he undertook a posting to the then Studies Guidance Group at DST Group Headquarters in Canberra. Geoff is currently the manager of AD's F/A-18 Flaw IdeNtification through the Application of Loads (FINAL) centre barrel-testing program.*

---

*This page is intentionally blank.*

# Contents

*This page is intentionally blank.*

# 1. Introduction

Full-scale fatigue tests (FSFTs) are conducted for the Royal Australian Air Force (RAAF) to support the structural integrity management plans of their various fleets [1 2]. Loads that simulate flight are applied to the airframe to generate representative fatigue damage that would be expected in service. Such tests are typically conducted to validate the design safe life, or determine when and where structural failure will occur. Information such as critical crack sizes and failure modes can be ascertained to support engineering analyses, which in some cases may even assist in the development of service life extension strategies [3].

Structural integrity management relies heavily on strain measurements taken during FSFTs. These are generally recorded at multiple points across the airframe, including regions of low stress gradient as well as high density spatial recordings in regions of high stress gradient at known hot spots and areas of interest. Large and/or complex structures may have thousands of strain sensing points, providing detailed data on the fatigue damage profile of the aircraft. FSFT strain results are also used directly to perform structural calculations, compare against flight test data, or verify finite element model predictions.

The industry standard method of measuring strain has been to use electrical resistance foil strain gauges (FSGs). This measurement technique is well established and has been in use for decades [4]. However, the installation of FSGs for detailed strain surveys can be both complex, time consuming, resource intensive and costly.

Generally, three shielded wire cables are required per FSG to connect to the resistance measurement system. This becomes a major installation issue when there are thousands of sensing points across an airframe. These shielded wire cables add an additional layer of complexity to the installation of FSGs; occasionally additional gantries are needed to route the thousands of wire cables as shown in Figure 1. This electrical wiring also adds non flight-representative weight to the structure and can obstruct non-destructive inspections of the airframe under test.

Optical fibre based sensing systems present the opportunity to significantly reduce installation complexity and weight since strain sensing is distributed along one optical fibre with a cross section approximating the dimensions of a human hair. These sensing systems are insensitive to EMI, fatigue and corrosion resistant and do not require ongoing calibration.

There are many fibre optic strain measurement systems that are currently commercially available for both discrete and distributed sensing. In particular, significant advances have been made in recent years in the use of Rayleigh scattering in optical fibres to measure strains [5]. This report documents the experimental evaluation of a commercially available distributed strain and temperature measurement system based on Rayleigh scattering in optical fibres. The aim of the evaluation was to assess the suitability of the technology as an alternative to conventional electrical resistance foil strain gauges for the measurement of strains on full-scale fatigue testing of Defence platforms. The system under evaluation was the ODiSI-B version 4 developed by Luna Innovations Incorporated for distributed strain and temperature measurements with a high spatial resolution at acquisition speeds up to 250 Hz.


*Figure 1: Aft view of an F/A18 fuselage undergoing fatigue testing at DST Group with overhanging support gantry to support the FSG electrical wiring.*

# 2. Background

## 2.1 Optical Fibre Based Strain Sensing

Optical fibre based strain sensors have been available for many years and are a potential alternative to FSGs. Optical fibres do not have the same electrical or mechanical drawbacks as FSGs. A single optical fibre can multiplex multiple sensing points along the fibre, which reduces the connection and installation issues that are inherent to most FSGs for broad area measurements. Fibre optic sensors can be broadly classified into two main types; discrete or distributed. Discrete sensors rely on transducers incorporated into the optical fibre at discrete locations that provide a reading of the strain experienced by the optical fibre at that point, thus providing a pseudo-distributed strain measurement. Truly distributed fibre optic strain sensors rely on the material properties of the fibre itself. Here, the entire fibre acts as the sensor and changes to the back-scattered light are used to characterise the strain experienced by the fibre. Further details about each of these strain sensor classes are given in the proceeding sections.

### 2.1.1 Discrete Fibre Optic Strain Sensors

The two main types of discrete fibre optic strain sensor are Fibre Bragg Gratings (FBGs) and Fabry-Perot (F-P) cavity based sensors.

FBGs are the most common type of discrete strain sensor [6]. A fibre Bragg grating is a periodic change in refractive index written into the core of an optical fibre. Bragg gratings are designed to reflect light travelling down the core of the optical fibre at a specific wavelength determined by the period of the index modulation. When the fibre is stretched or compressed the period of the index modulation changes and hence so does the wavelength of the reflected light.

The equation governing this relationship is defined as;

$$\lambda_B = 2n\Lambda \qquad [1]$$

where $\lambda_B$ is the peak wavelength of the reflected light, n is the effective refractive index of the fibre and $\Lambda$ is the pitch of the grating. Multiple gratings designed to reflect light at different wavelengths can be written into a single optical fibre as represented schematically in Figure 2 providing an effective way to achieve high density distributed strain sensing without the requirement for complex wiring.

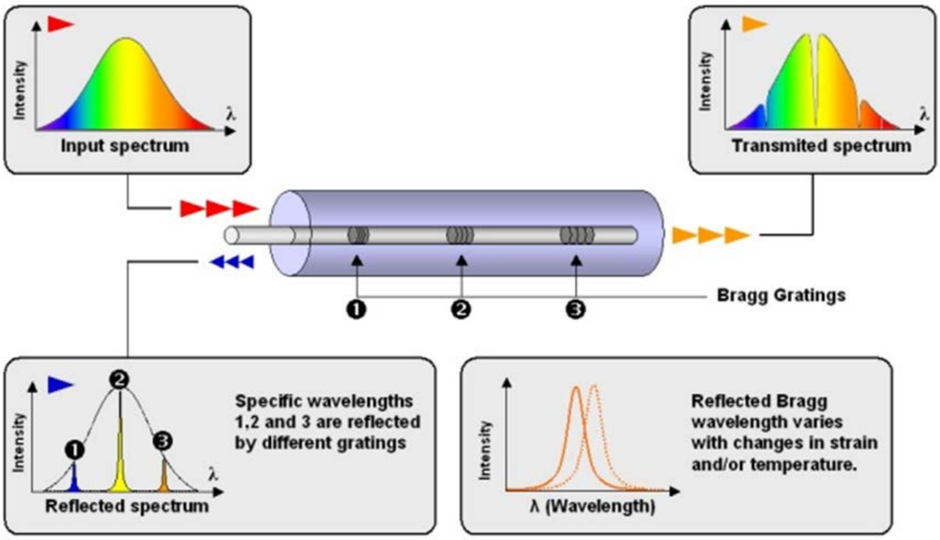


*Figure 2: Schematic diagram demonstrating the principle of operation of Bragg grating sensing using Wavelength Division Multiplexing (WDM).*

Fabry-Perot based strain sensors rely on a cavity or gap incorporated into the fibre. This sensor measures strain by determining the cavity length variation using an interferometric interrogation technique [7]. F-P based sensors generally have a wider operating temperature range than FBGs but they are not as easily multiplexed which makes them less attractive for multi-point measurements of strain.

### 2.1.2 Fibre Optic Distributed Strain Sensors

Distributed fibre optic sensing relies on the principle that every optical fibre has a unique scattering signature based on its material properties. This scattered signal remains constant in the absence of external factors. Changes in strain and/or temperature along the optical fibre cause changes to the fibre's material properties influencing its scattering signature within this region. These changes in scattered signal can be quantified to provide a distributed measurement of strain. The three main scattering mechanisms which may be interrogated to provide a measure of strain are Rayleigh, Brillouin and Raman [8].

Scattering-based measurement systems have been commercially available for some time, mainly relying on Raman or Brillouin scattering. Optical Time Domain Reflectometry (OTDR) is a common way to interrogate the fibres for Brillouin and Raman scattering. There are different variants on this method but the basic principle is the same. OTDR uses the time of flight of the back-scattered light to determine the location of the strain. These systems allow distributed measurements over long distances (up to kilometres) but tend to have poor spatial resolution and long acquisition times. Typical field applications for these systems include pipeline monitoring and structural health monitoring of large-scale infrastructure such as roads and bridges.

Rayleigh scattering usually provides a stronger back scattered signal which allows interferometric interrogation techniques to be employed. Inteferometry allows higher sampling rates with better spatial fidelity but the coherence length of the source laser (metres) limits the sensor length. These faster systems are inherently more suited to full-scale fatigue testing where the strain response to dynamic loading is often required.

# 3. Odisi B: System Outline

The ODiSI-B version 4 by Luna Innovations is a commercially available distributed strain measurement system based on Rayleigh scattering. The basic operating principle of the ODiSI-B system is the use of Optical Frequency Domain Reflectometry (OFDR) combined with a Mach Zehnder interferometer to characterise the Rayleigh scattering. Using these elements in tandem enables a relatively high sampling rate and increased spatial resolution. The system can provide both static and dynamic measurements with sampling rates up to 250 Hz over sensing lengths up to 20 metres as outlined in Appendix A.

Within the ODiSI-B the light initially splits in a 90:10 ratio into the main Mach-Zehnder interferometer and a trigger interferometer used to compensate for any nonlinearity in the laser tuning as shown in Figure 3. In the main Mach-Zehnder interferometer the light is split again 50:50 to a reference and sensor arm.

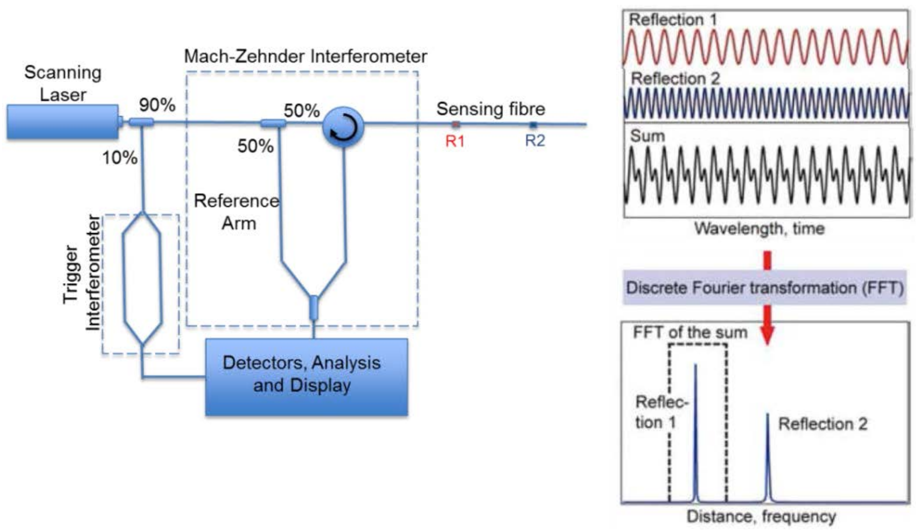


*Figure 3: Schematic diagram showing the principle of operation of the Luna ODiSI-B system.*

The light scatters in all directions but a small portion is backscattered. Observing the response from two arbitrary locations along the fibre R1 and R2 as shown in Figure 3, the backscattered light interferes with the light sent along the reference arm creating interference fringes. The frequency of the resulting backscattered interference fringes provide the location of the signal along the fibre. These frequencies are windowed, with the range of frequency window directly proportional to the sensor gauge length. An inverse Fourier Transform is then applied to each frequency window, giving a unique fluctuating intensity profile for the unstrained fibre as shown in Figure 4. This pattern is characterised prior to shipment of the sensing fibre. Any changes in temperature or strain to the fibre will induce a frequency shift to this profile, which can be used to measure the temperature or strain.

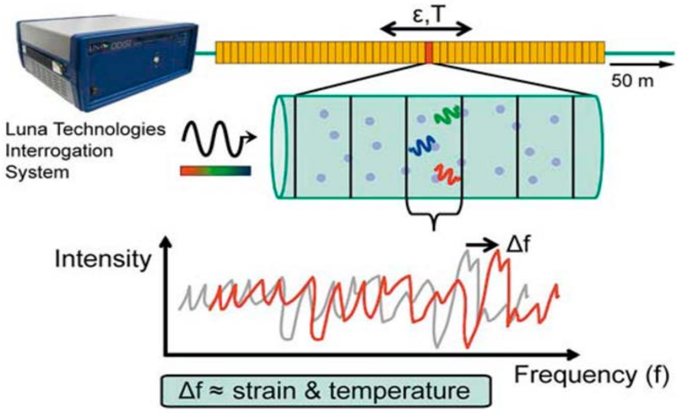


*Figure 4: Effect of strain or temperature on Rayleigh backscatter for a particular frequency window (Image courtesy of Luna Innovations).*

### 3.1.1 Specifications Of Odisi System

The Luna ODiSI –B system can be supplied with several sensing resolutions and sampling frequencies as outlined in Appendix A. One option comes supplied as standard and additional measurement modes are provided as software options. The standard and high resolution modes of operation were evaluated as part of this study.

The standard mode has gauge lengths of 5.12 mm measured in 2.56 mm intervals with an acquisition rate of up to 100 Hz. The higher resolution mode has gauge lengths of 1.28 mm measured at 0.64 mm intervals with a maximum acquisition rate of 23.8 Hz. Any test that requires both resolution modes must be run twice so that the data can be acquired in each mode. Each individual sensing fibre is supplied with a USB flash drive containing the scattering profile for the unstrained fibre, which is used as a baseline for the measurement.

There are two ways to analyse the reflected back scatter. ***Live processing*** acquires and processes the data "on the fly" providing a real-time measurement of strain. The other alternative is to record the back scattered signal for ***post processing*** at a later date. There are pros and cons to each method of data processing.

The rate at which the data can be processed live is limited by the hardware and depends on the size of the data stream. Thus, it becomes a compromise between resolution and fibre length as shown in Table 1 but the sampling rate is typically significantly less than the maximum rate specified by the manufacturer. The post–processed data can be acquired at the maximum speed indicated by the system specifications but the file sizes for the unprocessed data are very large as indicated in Table 2, rendering them impractical for long-term studies.

*Table 1: Sampling rates for different lengths, resolution and types of sampling rates.*

| Length (metres) | Resolution mode | Live sampling rate (rounded to closest Hz) | Post processed sampling rate |
|---|---|---|---|
| 1 | High | 8 Hz | 23.8 Hz |
| 1 | Standard | 33 Hz | 100 Hz |
| 2 | High | 5 Hz | 23.8 Hz |
| 2 | Standard | 20 Hz | 100 Hz |
| 5 | High | 2 Hz | 23.8 Hz |
| 5 | Standard | 8 Hz | 100 Hz |
| 10 | High | 1 Hz | 23.8 Hz |
| 10 | Standard | 5 Hz | 100 Hz |

*Table 2: Size of files and compilation time for Post Processing 1 minute of sampling data.*

| Length (meters) | Resolution mode | odb file size (kB) | txt file size (kB) | Compile time (secs) | Number of scans |
|---|---|---|---|---|---|
| 10 | High | 3 809 488 | 181 352 | 1174 | 1446 |
| 10 | Standard | 4 229 126 | 193 677 | 1214 | 5919 |
| 5 | High | 3 772 605 | 94 463 | 606 | 1432 |
| 5 | Standard | 4 282 714 | 95 791 | 654 | 5994 |
| 2 | High | 3 772 605 | 37 869 | 270 | 1432 |
| 2 | Standard | 4 312 723 | 38 961 | 307 | 6036 |
| 1 | High | 3 767 336 | 20 711 | 157 | 1430 |
| 1 | Standard | 4 292 717 | 23 553 | 189 | 6008 |

# 4. Experimental Qualification: Coupon Testing

## 4.1 Determination of Minimum Fibre Bend Radius

Prior to any performance evaluation of the Luna ODiSI-B system, a preliminary experiment was conducted to investigate the effect of fibre curvature on optical loss of the system. The purpose of this experiment was to determine the minimum fibre bend radius that could reliably be accommodated in a measurement system without compromising signal integrity. The test article was a 0.8 mm thick 4-ply carbon fibre panel (Hexcel M18 prepreg) with a 0°, +45°, -45°, 0° lay-up. Polyimide (Kapton) tape was used to attach a 1 m long optical fibre to the surface of the composite plate in a curved geometry as shown in Figure 5(a).

The panel was clamped to the bench at one end with a weight placed on the far end to provide a cantilevered loading arrangement. This loading arrangement induced a monotonically decreasing strain gradient along the length of the fibre from the clamp region to the far end of the plate. Nine strain regions from the fibre (three along each sensing line) were monitored as indicated by the dots in Figure 5.

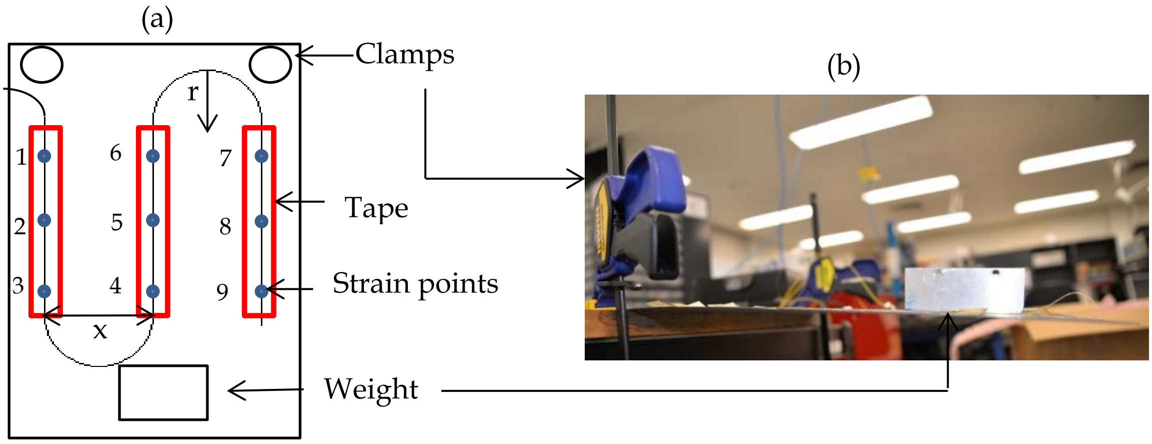


*Figure 5: (a) Schematic lay-up of fibre on the composite plate; (b) Side-view of cantilevered plate loading arrangement.*

The distance between the parallel lines of the fibre (x) was reduced from 50 mm to 10 mm in 10 mm steps, giving a radius of curvature (r) from 25 mm to 5 mm. At each distance, a strain measurement from the nine points indicated in Figure 5 was taken using both the high and standard resolution modes.

Figures 6(a) and (b) shows the dynamic response from the second measurement point for the high and low-resolution measurement modes over a 60-second measurement interval. All the measurements were taken with the beam loaded with the exception of the 5 mm radius geometry where the measurement was taken unloaded.

The results confirm that strain measurements were possible without any loss of data or discernible increase in noise in both high and standard resolution measurement modes for all radii tested up to a minimum curvature radius of 5 mm. This implies that the sensing fibre should be able to operate when routed in complex geometries requiring small bend radii. There was a larger overall noise level observed on the higher resolution measurements as compared to the lower resolution measurements associated with the smaller scattered signal from the shorter measurement interval.

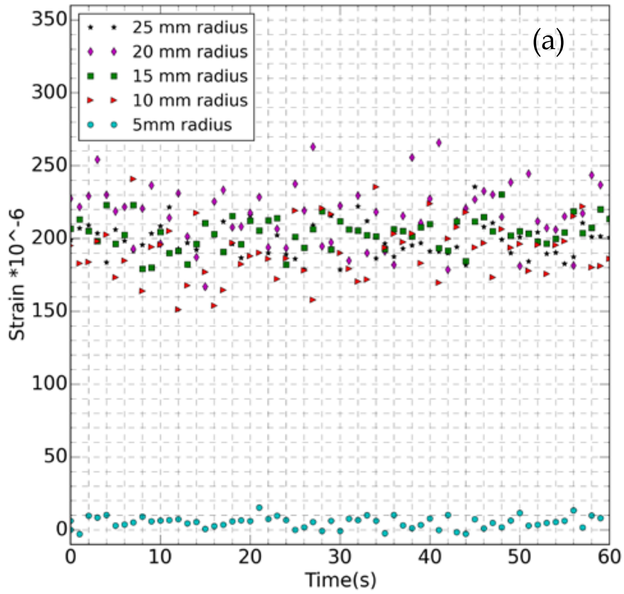


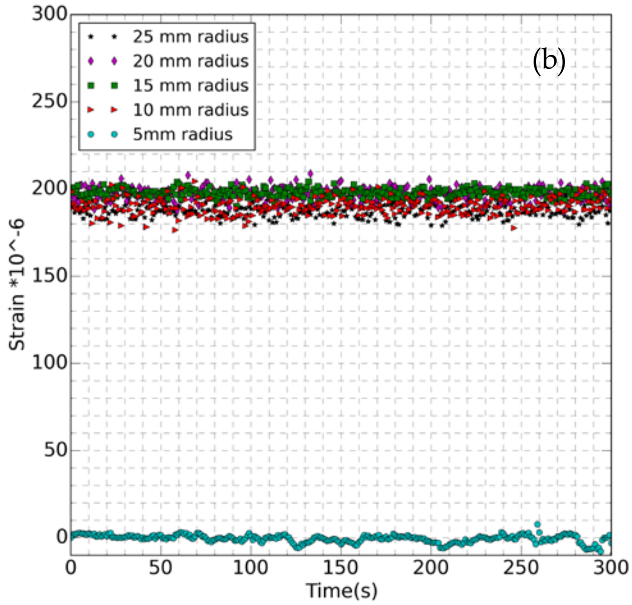


*Figure 6: Dynamic response from the second measurement region for (a) high and (b) low resolution measurement modes over a 60-second measurement interval.*

## 4.2 Characterisation of Response to Strain Gradients

The next experiment compared the performance of the Rayleigh system against a series of of FSG arrays for the measurement of a strain gradient. The test article was an aerospace grade aluminium (2024-T3) coupon measuring approximately 4 mm thick by 100 mm wide by 400 mm long with a through thickness hole of 20 mm in diameter at the centre as shown in Figure 7 (a). Figure 7(b) shows the strain distribution along the y-axis predicted by the Finite Element Analysis (FEA) for the coupon at a representative loading. The strain-sensing axis was aligned with the long edge of the coupon. Six strips, in two sensing lines, of Kyowa KFG-1-120-D9-11N10C2 FSGs, each strip comprising of five 1 mm long sensing elements, were adhered to the RHS of the hole and a 2 m optical fibre bonded in 6 parallel sensing lines was adhered to the LHS of the hole as indicated in Figure 7(c) and 8.

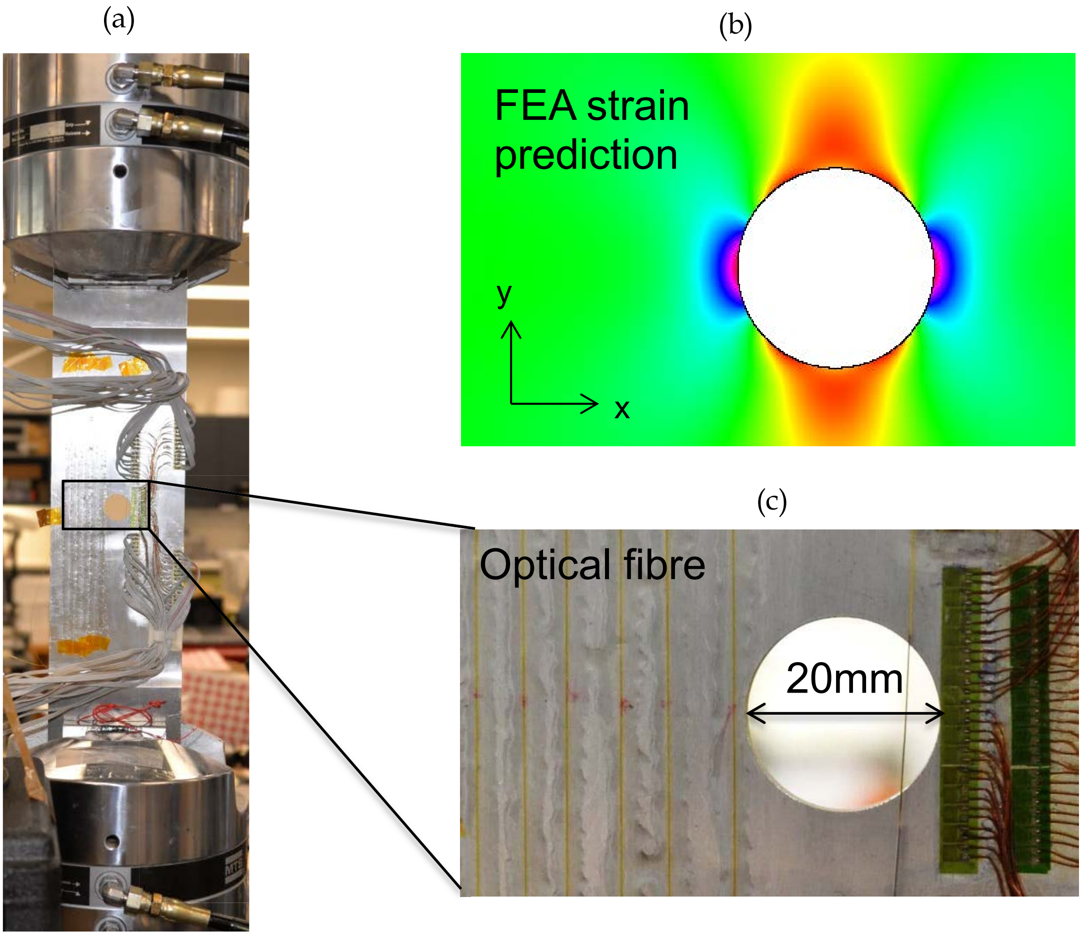


*Figure 7: (a) Aerospace grade aluminium (2024-T3) coupon under tensile loading in a mechanical test machine; (b) FEA model of strain distribution along y axis; (c) Close-up image showing detail of optical and electrical strain sensors around the hole.*

The optical fibre was arranged into 6 parallel bonded lines each 180 mm in length that gave 421 sensing points in standard resolution mode and 1687 in high-resolution mode.

On the other side of the hole, 30 FSGs in six 5-gauge strips were arranged into two shorter parallel lines mirroring the distance from the hole of the first two optical fibre-sensing lines. The active gauge length of each FSG was 1 mm with a sensor footprint of 1 mm by 1.4 mm and the pitch between successive gauge centre points was 1 mm.

The same surface preparation was used prior to attachment of both the FSGs and the optical fibre (de-greasing followed by light abrasion and cleaning).The FSGs were attached using a standard general-purpose strain gauge adhesive (Vishay Micro-Measurement, M-Bond 200) and the optical fibre was attached using a UV curable adhesive (Norland Optical Adhesive, NOA-61) [9 10].

Kapton tape was used to pre-tension and hold the optical fibre in place temporarily prior to bonding and a Dino-Lite Digital Microscope and vernier calipers were used to assist in positioning the fibre to mirror the location of the FSGs. The first 10-20 mm of the sensing fibre was not bonded as it is important that this section of the fibre remains unconstrained to assist with the vibration correction algorithm implemented by the software.

A small paintbrush was used to apply the NOA-61 along the length of the optical fibre using several light applications to build up the adhesive to just cover the optical fibre. The primary direction of application was along the fibre, but brush strokes were also applied at a shallow angle relative to the substrate and perpendicular to the direction of the fibre to ensure a uniform bond line underneath the optical fibre. A broad area Maxima ML-3500 S UV-A lamp was used to cure the adhesive for approximately 2-3 hours.

Table 3 shows the final position of the optical fibres and FSGs relative to the edge of the hole as measured by the digital microscope after curing. It should be noted that although the second optical fibre line was 200 microns closer to the hole than the corresponding FSG the strain field experiences a much smaller gradient in this region and so a reasonable comparison can still be made.

*Table 3: Sensor position relative to edge of the hole*

| | **Line 1** | **Line 2** | **Line 3** | **Line 4** | **Line 5** | **Line 6** |
|---|---|---|---|---|---|---|
| **FSG** | 1.1 mm | 8.3 mm | N/A | N/A | N/A | N/A |
| **Optical Fibre** | 1.1 mm | 8.1 mm | 13.1 mm | 18.9 mm | 23.5 mm | 28.6 mm |

A hydraulically actuated uni-axial test machine, with a 50 kN capacity, was used to apply static loading according to the loading schedule in Table 4. Whilst setting up the specimen in the test machine care was taken to align the specimen perpendicular to the loading grips to ensure symmetric loading on either side of the hole.

At each loading interval the strain experienced by the optical fibre was measured using the ODiSI B in both high and low resolution modes. The FSG acquisition system utilised a National Instruments Ethernet chassis (NI cDAQ-9188XT) incorporating three quarter-bridge 120Ω strain modules (NI 9235) to give a total of 24 strain channels. The strain measurements were recorded on a PC from the NI cDAQ-9188XT via an Ethernet connection.

*Table 4: Static loading schedule for the measurement of strain*

| Load (kN) | Number of optical sensing points (high resolution) | Number of optical sensing points (low resolution) | Number of FSG sensing points |
|---|---|---|---|
| 0 | 1687 | 421 | 30 |
| 2 | 1687 | 421 | 30 |
| 4 | 1687 | 421 | 30 |
| 8 | 1687 | 421 | 30 |
| 12 | 1687 | 421 | 30 |
| 16 | 1687 | 421 | 30 |
| 20 | 1687 | 421 | 30 |

In addition to the static loading measurements, the coupon was cyclically loaded to a peak load of 16 kN at 5 Hz and the full-field stress distribution measurement around the hole was achieved using thermoelastic stress analysis (TSA). The primary purpose of the TSA scan was to confirm that the coupon was symmetrically loaded.

Figure 8 shows a schematic diagram of all the sensor locations on the aluminium coupon.

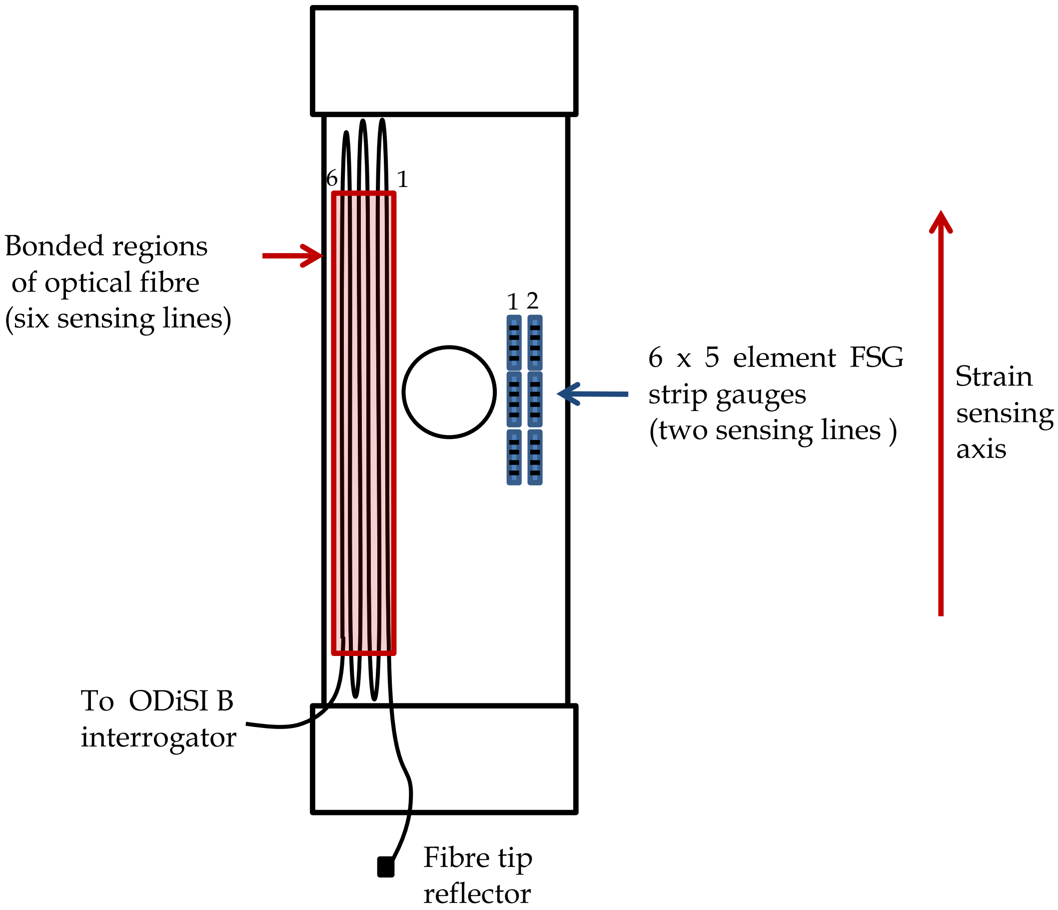


*Figure 8: Schematic drawing showing locations of strain sensors on the aluminium coupon.*

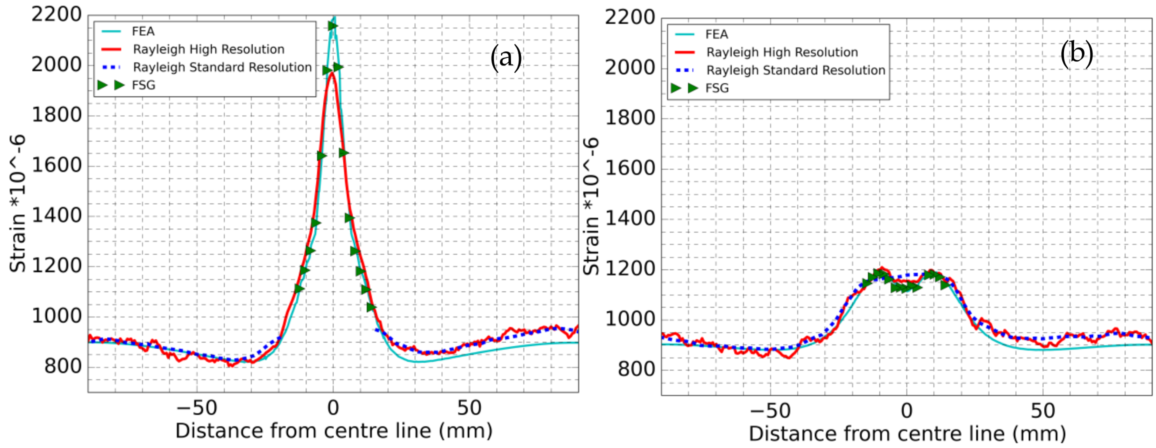


*Figure 9: (a) Strains along Line 1 of the aluminium coupon as predicted by the FEA and measured by the FSGs and both Rayleigh modes at 20 kN; (b) Strains along Line 2 of the aluminium coupon as predicted by the FEA and measured by the FSGs and both Rayleigh modes at 20 kN.*

Figure 9 (a) and (b) shows the response of all the sensors and FEA model along line 1 and line 2 respectively. The FSG measurements are indicated by the individual markers, the model predictions and the optical fibre measurements are plotted as continuous strain distributions.

The first major feature to note in Figure 9 (a) is that there is no data recorded by the optical fibre in standard resolution mode in the region close to the edge of the hole where the strain gradient is largest. One of the main assumptions for the ODiSI B system is that the strain across a gauge length is uniform. If this assumption is violated it is difficult to cross-correlate the scattered reflection spectra between the strained and unstrained fibre. There is a cross correlation threshold set in the software algorithm. As the signal to noise ratio approaches this threshold the data will start to drop-out.

An additional experiment was performed to determine the limits of the standard resolution mode to measure strain gradient. This test measured the strain distribution in standard resolution mode along line 2 as the applied load was incremented in 2 kN steps. The resultant strain distributions are shown in Figure 10. For the lower loads where the strain difference between successive measurement points was reasonably small, the strain values were calculated reliably by the ODiSI B system. As the load increased the strain data in the high gradient region began to destabilise (when the strain difference between the measurement points approached approximately 100 με) as shown in Figure 10 (b). Once the strain difference between measurement points had increased beyond 150 με the measurement data had completely dropped out as shown in Figure 10 (e). These values are broadly consistent with advice received during correspondence with the manufacturer on this issue.

By comparison, the high resolution mode has not dropped out over the same strain gradient. The gauge length for the high resolution mode is much shorter (1.28 mm as opposed to 5.12 mm for the standard mode), thus the strain difference is not as large within the measurement region. However, having smaller gauge lengths gives a higher noise level as shown in Figures 6 and 9.

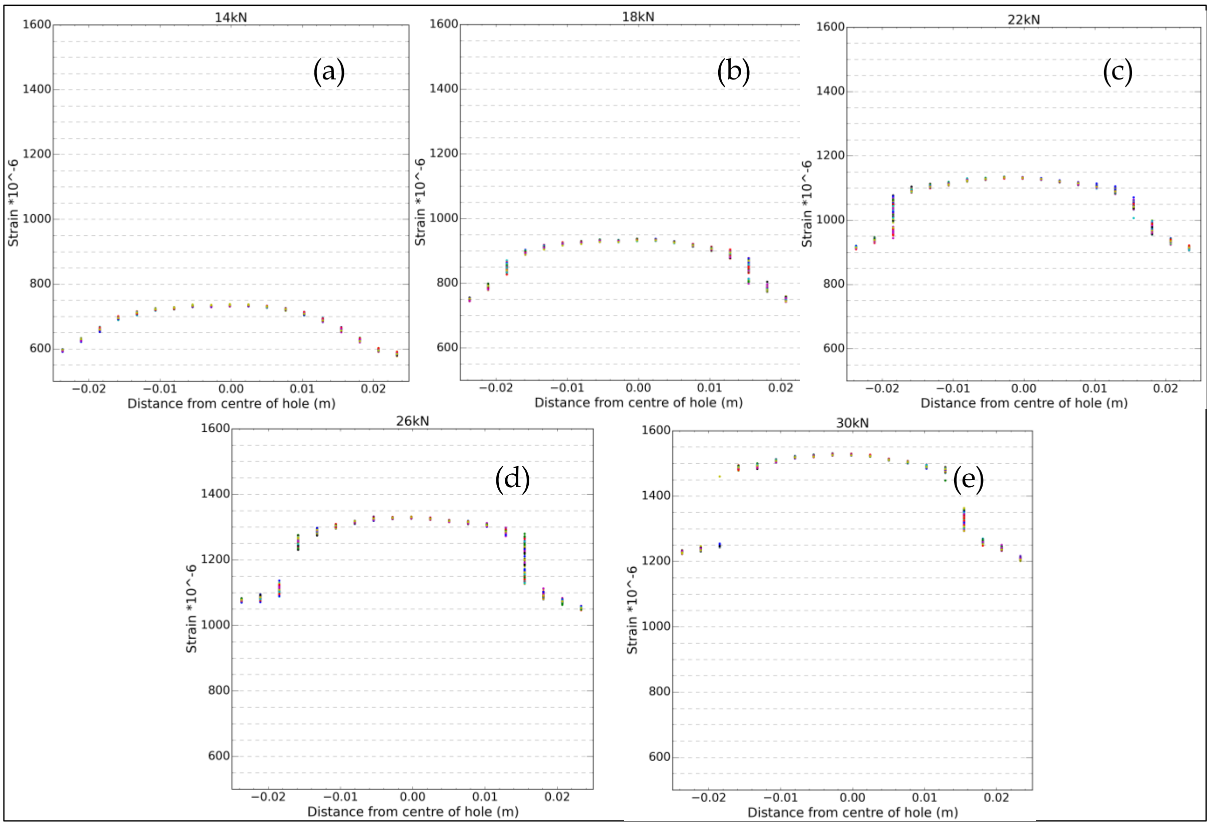


*Figures 10: (a)-(e) Response of optical fibre along sensing line 2 to incremental loading from 14kN to 30kN. Five sets of measurement data are shown at each load.*

Another feature to note with the data recorded in the standard resolution mode is that local strain features may be lost. This is effectively demonstrated along sensing line 2 as shown in Figure 9 (b) where the local dip in strain at the centre of the hole is not resolved by the optical measurement system when measuring in standard resolution mode.

The final discrepancy between the data sets in Figure 9 is the underestimation of the peak strain by approximately 10% by the optical system measuring in high resolution along sensing line 1. The TSA scan data was analysed and confirmed symmetric loading as shown in Figure 11, thus the discrepancy could not be attributed to asymmetric strain distributions between the RHS and LHS of the hole.

The analysis of the strain gradient data in the standard resolution mode (Figure 10) showed in regions of high strain gradient, prior to drop-out of the data, there was greater spread and reduced accuracy of the strain data. Correspondence from the manufacturer indicated that this threshold was approximately 500 με (across 1.28 mm) for the high resolution mode. The strain difference predicted by the model in this region was 520 με, so this was likely to be the reason for the underestimation of the strain data in this region. Both the experimentally measured and theoretically predicted strain at the centre of the hole where there is a high strain gradient was plotted against applied load as shown in

Figure 12. This data shows an increase in the discrepancy between the optically measured strain and model predictions as the load increased.

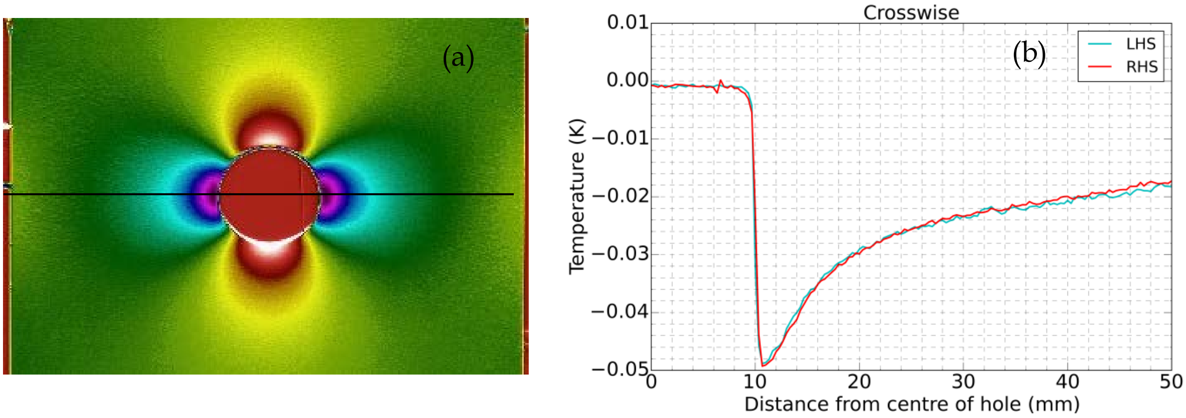


*Figure 11: (a) TSA scan of aluminium coupon in region around hole; (b) Comparison of temperature distributions on the RHS and LHS of the hole.*

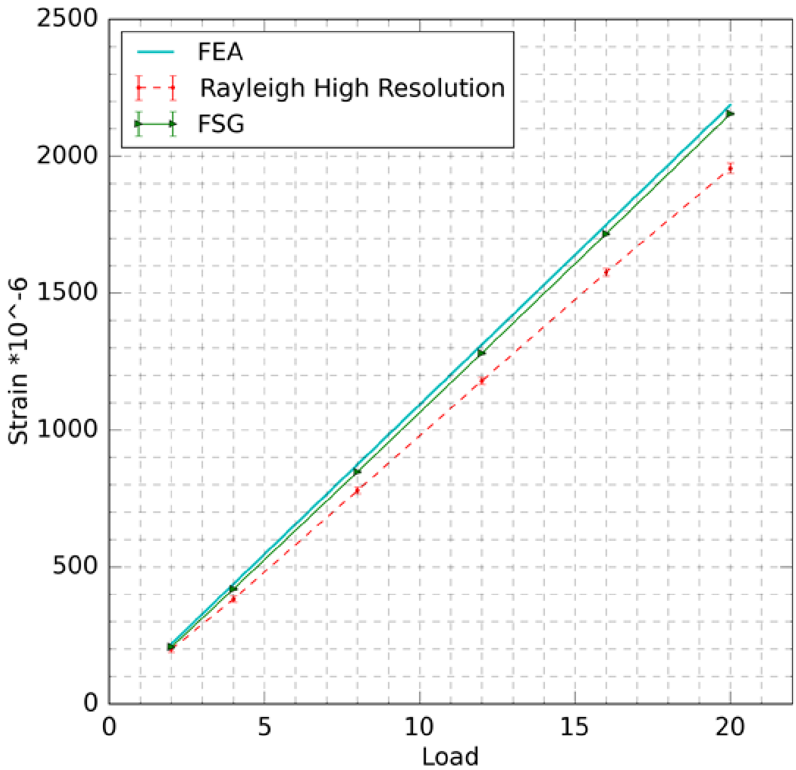


*Figure 12: Measured peak strain along sensing line 1 as a function of applied load.*

## 4.3 Response to Crack Propagation

The ability to detect and track crack growth during FSFTs is a key aspect of the testing process. Early detection allows the crack growth to be characterised prior to structural failure that can assist in structural management of the aircraft component.

The strain field induced by a crack, especially around the crack tip, tends to be highly localised. Hence, FSGs tend to detect the crack only if they are located in close proximity to it. If the crack propagates under or in close proximity to a FSG, this is usually indicated by a failure of the gauge. The purpose of this experiment was to understand the response of the optical strain measurement system to a crack in close proximity to the fibre and as the crack propagates underneath the fibre.

The same aluminium test coupon was used with a small notch introduced using a microfile at the edge of the hole on the optical fibre side (see Figure 13) to initiate crack growth. The coupon was cyclically loaded in tension at 5 Hz starting at a peak load of 1 kN according to the loading schedule shown in Table 5 to initiate stable crack growth. Once the crack had initiated the applied load was reduced back to a 6 kN load span and then gradually increased to a point at which the crack propagation rate was slow and stable (14 kN load span). Measurements were then taking using the ODiSI B Rayleigh system in high and low resolution after each loading block at the static load of 15 kN. A digital microscope (Dino-Lite) located on the same (front) side as the optical fibre was used to measure the crack length and a TSA scan (using a FLIR A35 Microbolometer camera and MiTE analysis software) was also taken on the non-instrumented (back) side of the specimen to provide an alternate method to track the crack initiation and propagation.

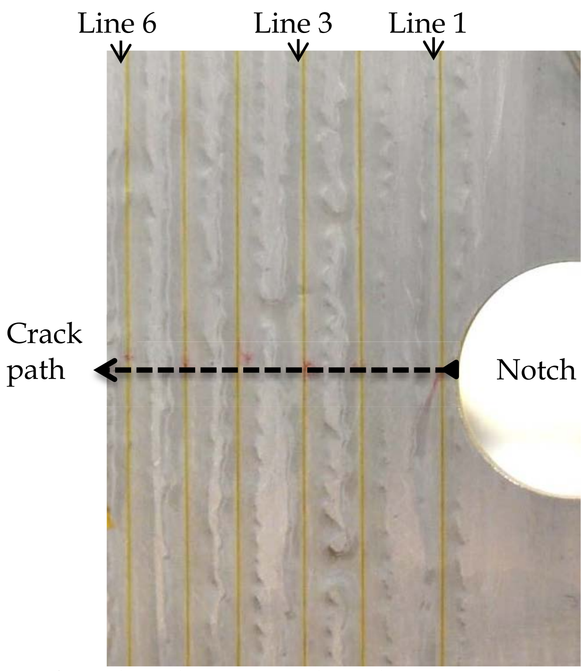


*Figure 13: Location of notch and anticipated crack propagation path.*

*Table 5: Coupon tensile loading schedule at 5 Hz starting from a peak load of 1 kN to achieve crack initiation and stable crack growth.*

| Load span (kN) | Number of tests | Cumulative test number | Number of blocks per test | Notes |
|---|---|---|---|---|
| 2 | 1 | 1 | 120 | |
| 4 | 1 | 2 | 120 | |
| 6 | 1 | 3 | 120 | |
| 8 | 1 | 4 | 120 | |
| 10 | 1 | 5 | 120 | |
| 12 | 1 | 6 | 120 | |
| 14 | 1 | 7 | 120 | |
| 15 | 1 | 8 | 120 | |
| 16 | 1 | 9 | 120 | |
| 17 | 1 | 10 | 120 | |
| 18 | 1 | 11 | 120 | |
| 19 | 1 | 12 | 120 | |
| 20 | 1 | 13 | 120 | |
| 20 | 6 | 19 | 120 x 4/100 x 2 | |
| 6 | 3 | 22 | 200 x 1/127 x 1/500 x 1 | Reduced loading to ensure slow and stable crack growth |
| 7 | 5 | 27 | 200 | |
| 8 | 5 | 32 | 150x4/100x1 | |
| 9 | 3 | 35 | 120 | |
| 10 | 4 | 39 | 120 | |
| 11 | 3 | 42 | 120 | |
| 12 | 3 | 45 | 120 | |
| 13 | 3 | 48 | 120 | |
| 14 | 1 | 50 | 120 | |

Table 6 shows the results for the measured crack length after each loading interval. The crack length was measured at the front of the coupon (on the same side as the optical fibre) using the digital microscope. The crack length was also measured on the back side of the coupon using TSA with the coupon hole used to scale the measurement. Figures 15, 16 and 17 show the strain distribution as measured by the optical fibre for the three crack positions shown in Figure 14. Only the data from the high resolution measurement is displayed as the standard resolution measurement mode was not able to resolve the strain gradient caused by the crack.

*Table 6: Crack length vs load block number as measured by the digital microscope on the front (sensor) side and the TSA scan (back side).*

| Test No. | Blocks per test | Length of crack sensor side (mm) | Length of crack IR camera side (mm) | Test No. | Blocks per test | Length of crack sensor side (mm) | Length of crack IR camera side (mm) |
|---|---|---|---|---|---|---|---|
| 50 | 120 | 0.285 | 0.328 | 84 | 60 | 12.522 | 12.772 |
| 51 | 120 | 0.387 | 0.408 | 85 | 60 | 12.868 | 13.204 |
| 52 | 120 | 0.41 | 0.622 | 86 | 60 | 13.174 | 13.511 |
| 53 | 120 | 0.569 | 0.901 | 87 | 61 | 13.82 | 13.906 |
| 54 | 120 | 0.669 | 1.207 | 88 | 60 | 14.255 | 14.24 |
| 55 | 120 | 0.842 | 1.350 | 89 | 60 | 14.81 | 14.658 |
| 56 | 120 | 1.511 | 1.502 | 90 | 60 | 14.984 | 14.979 |
| 57 | 120 | 1.733 | 1.783 | 91 | 60 | 15.485 | 15.356 |
| 58 | 121 | 2.219 | 2.111 | 92 | 60 | 15.85 | 15.698 |
| 59 | 120 | 2.802 | 2.538 | 93 | 60 | 16.441 | 16.045 |
| 60 | 120 | 3.207 | 3.103 | 94 | 60 | 16.539 | 16.437 |
| 61 | 120 | 3.38 | 3.590 | 95 | 60 | 17.16 | 16.986 |
| 62 | 120 | 4.259 | 4.022 | 96 | 60 | 17.377 | 17.309 |
| 63 | 120 | 4.554 | 4.567 | 97 | 60 | 17.746 | 17.845 |
| 64 | 80 | 4.809 | 4.79 | 98 | 60 | 18.056 | 18.126 |
| 65 | 80 | 5.1 | 5.148 | 99 | 60 | 18.462 | 18.606 |
| 66 | 80 | 5.673 | 5.482 | 100 | 60 | 18.792 | 19.085 |
| 67 | 80 | 6.014 | 5.77 | 101 | 60 | 19.079 | 19.563 |
| 68 | 80 | 6.266 | 6.028 | 102 | 60 | 19.616 | 20.042 |
| 69 | 80 | 6.423 | 6.461 | 103 | 60 | 19.812 | 20.561 |
| 70 | 80 | 6.722 | 6.820 | 104 | 60 | 20.577 | 20.982 |
| 71 | 86 | 7.004 | 7.326 | 105 | 60 | 21.539 | 21.591 |
| 72 | 80 | 7.402 | 7.797 | 106 | 50 | 21.864 | 21.972 |
| 73 | 80 | 7.699 | 8.02 | 107 | 50 | 22.174 | 22.413 |
| 74 | 80 | 8.05 | 8.579 | 108 | 50 | 22.723 | 22.653 |
| 75 | 80 | 8.595 | 8.923 | 109 | 50 | 23.089 | 23.431 |
| 76 | 80 | 8.842 | 9.393 | 110 | 52 | 23.733 | 23.951 |
| 77 | 80 | 9.337 | 9.777 | 111 | 50 | 24.364 | 24.522 |
| 78 | 80 | 9.919 | 10.172 | 112 | 40 | 24.537 | 25.018 |
| 79 | 80 | 10.22 | 10.78 | 113 | 40 | 25.544 | 25.364 |
| 80 | 80 | 10.811 | 11.151 | 114 | 40 | 25.875 | 25.925 |
| 81 | 80 | 11.504 | 11.375 | 115 | 40 | 26.63 | 26.527 |
| 82 | 80 | 12.001 | 12.079 | 116 | 40 | 27.076 | 27.082 |
| 83 | 60 | 12.296 | 12.502 | 117 | 40 | 27.433 | 27.849 |

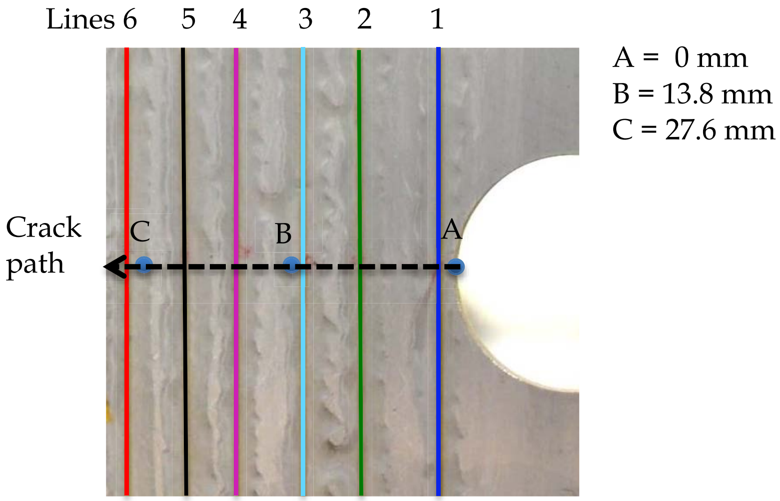


*Figure 14: Close-up photograph of the optical fibre, with the fibre lines coloured to match the strain distributions in Figures 15, 16 and 17 at crack locations A, B and C respectively.*

Figure 15 shows response to the uncracked coupon from both the high resolution mode and TSA. The TSA scan shows slight asymmetry on the LHS due to the notch. The optical fibres show a strain distribution consistent with the model predictions.

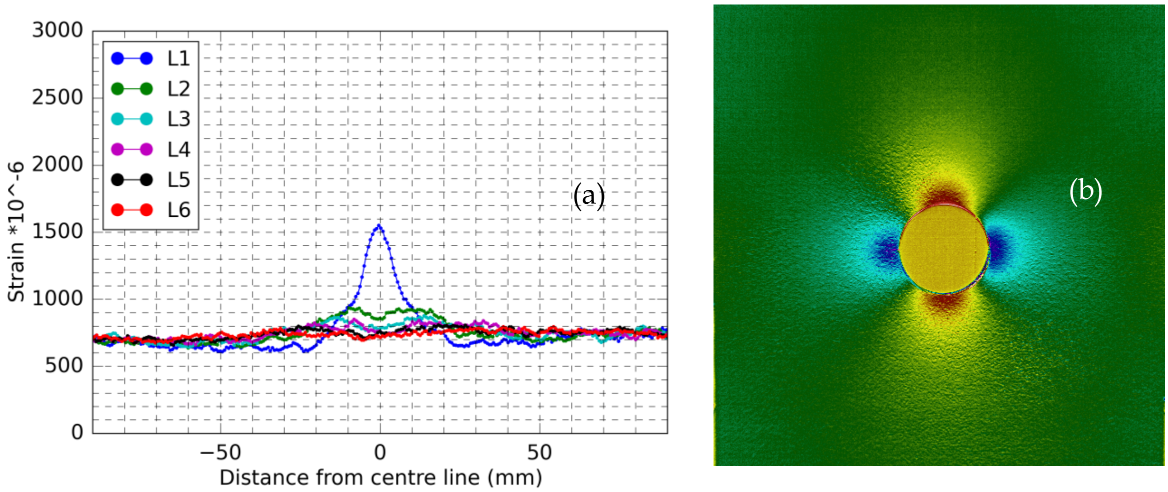


*Figure 15: (a) Strain distribution measured by the 6 fibre lines after notch applied (prior to crack initiation); (b) TSA scan of notched coupon at same point*

Figure 16 (a) shows the response of the optical fibres as the crack has progressed to the third sensing line. The data shows clearly the dropout from Lines 1 - 3 which are caused by the high strain gradients in the fibre as the fibre bridges the crack as it opens. The other important feature to note is that, although the data drops out in the region surrounding the crack, the signal integrity from the remainder of fibre remains intact. The inference from this result is that there is no physical damage induced in the fibre as the crack propagates beneath it. Lines 1 and 2 are also showing strain relief behind the crack tip which is consistent with the theory and is also observed in the TSA scan (Figure 16 (b)). Lines 4 to 6 also show a change in strain response to the undamaged state, with increasing strain near the crack tip detected by all fibres.

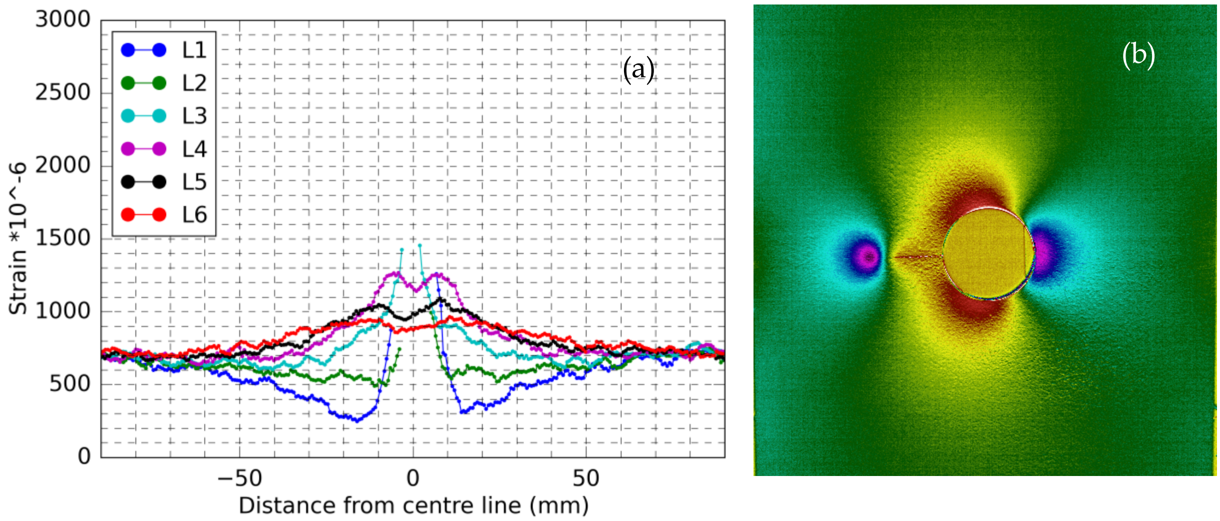


*Figure 16: (a) Strain distribution of 6 fibre lines after the crack has progressed to position B (13.8mm); (b) TSA scan of coupon at same point.*

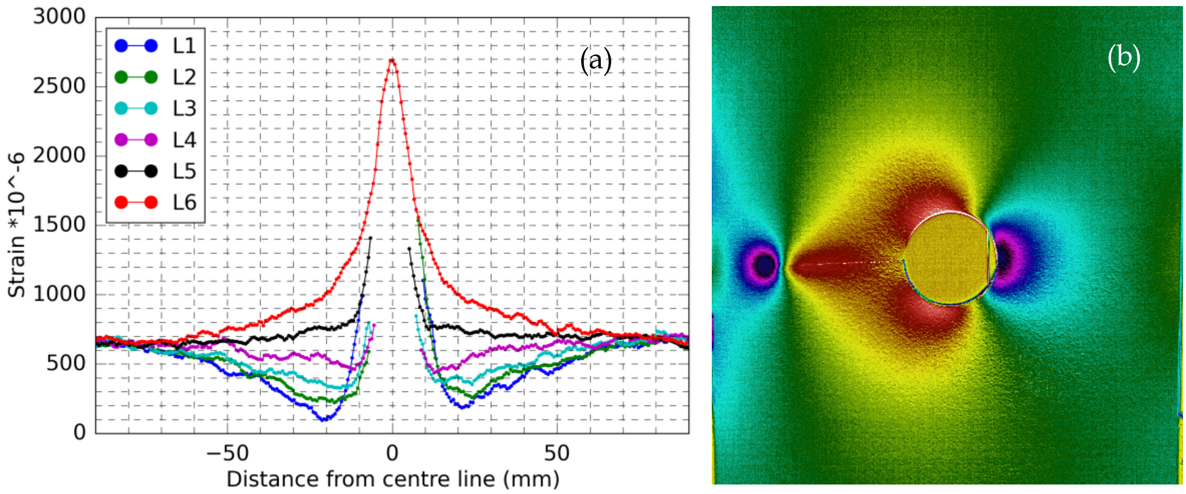


*Figure 17: (a) Strain distribution of 6 fibre lines after the crack has progressed to position C (27.6 mm); (b) TSA scan of coupon at same point.*

Figure 17 (a) shows the response of the optical fibres as the crack has progressed to approximately 1 mm before the sixth sensing line at a distance of 27.6 mm from the edge of the hole. At this point there is loss of data from all the fibres in the region where the fibre traverses the crack which is consistent with the predicted behaviour and previous evidence in regions of high strain gradient. The crack opening distance under load at line 1 was measured to be approximately 100 μm. The optical strain data in the far-field away from the region of the crack is still consistent with the model, showing that the optical fibre is still physically intact. The strain relief is now apparent in the first four sensing lines of the fibre.

# 5. Full Scale Fatigue Testing

## 5.1 Test Article

The test article used for the FSFT trial was an ex-service Classic Hornet F/A-18 centre barrel (CB). The CB designation was CB19 and the test forms part of a larger testing program for ex-service F/A-18 A/B/C/D aircraft investigating the fatigue life, damage mechanisms and failure locations of this component when subjected to simulated operational spectrum loading [11].

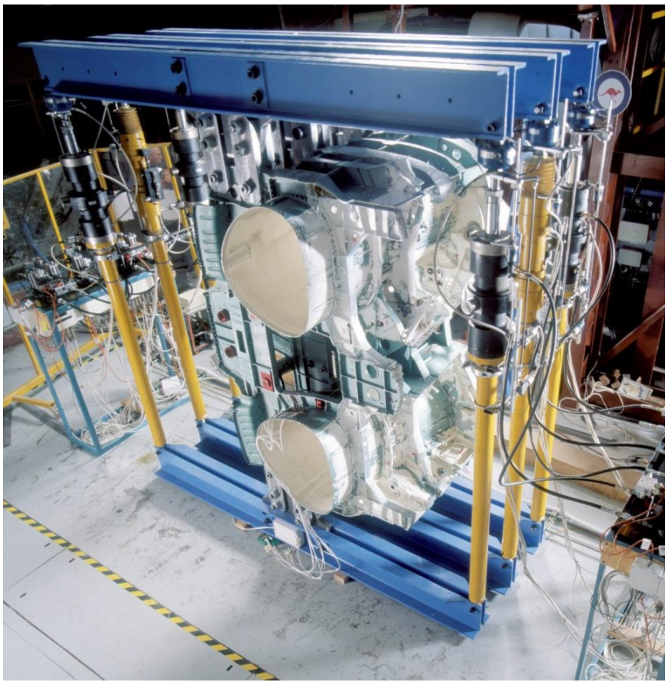

*Figure 18: Full-scale fatigue test rig with centre barrel installed and loaded at its wing mounting points.*

The CB is a key load bearing structure comprising of three centre fuselage bulkheads which transfer aerodynamic wing loads to the fuselage. The CB shown in Figure 18 is rotated 90 degrees from its nominal position and is housed in a test rig that applies Wing Root Bending Movement (WRBM) loads via frames connected to the wing attachment lugs on each of the three bulkheads. Figure 19 shows a schematic representation of the load actuation system identifying the hydraulic actuators and bulkheads.

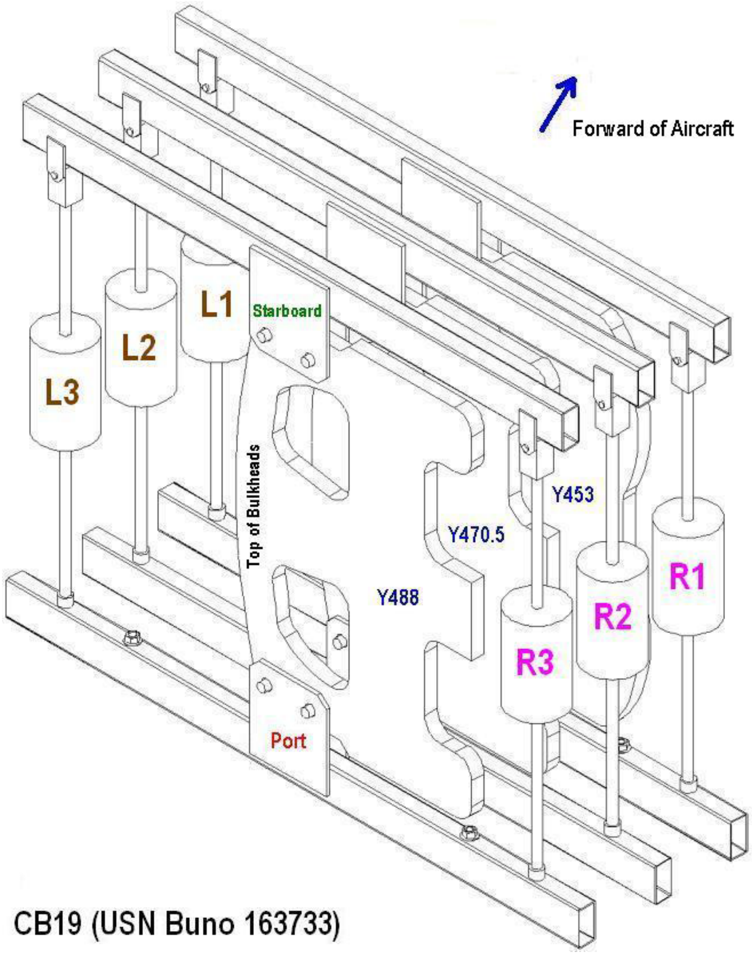


*Figure 19: Test rig schematic identifying actuators, bulkhead and orientations.*

## 5.2 FSFT-Discrete Testing

The first experiment on the FSFT compared the performance of a FSG and the Rayleigh optical system for the measurement of strain at a single approximately co-located point. An FBG strain sensor was also applied in close proximity to the other two sensors. The sensing location was on the lower flange of the portside centre bulkhead (Y470.5) as shown in Figure 20. The Y453 bulkhead had already failed and removed prior to the test.

The same surface preparation was used for all the sensors. All the protective coatings (paints and sealants) were removed and the surface was stripped back to bare aluminium in the region where the sensors were to be applied, followed by light abrasion and cleaning. The FSG was applied using a standard strain gauge adhesive (AE-10) according to standard procedures [9]. The Rayleigh scattering fibre and the optical fibre containing the FBG were bonded to the surface using a UV curable liquid photopolymer (NOA-61). The adhesive was applied using a small paintbrush and then exposed to UV light using a UV LED torch (OPTIMAX 365 UV). Both optical fibres had approximately 80 mm of fibre bonded to the component in order to avoid edge effects in the region of the sensor. The gauge length of the FBG was 5 mm and the gauge length for Rayleigh sensing fibre was 5.12 mm in standard resolution mode and 1.28mm in high resolution mode. The gauge length of the FSG was 2mm.

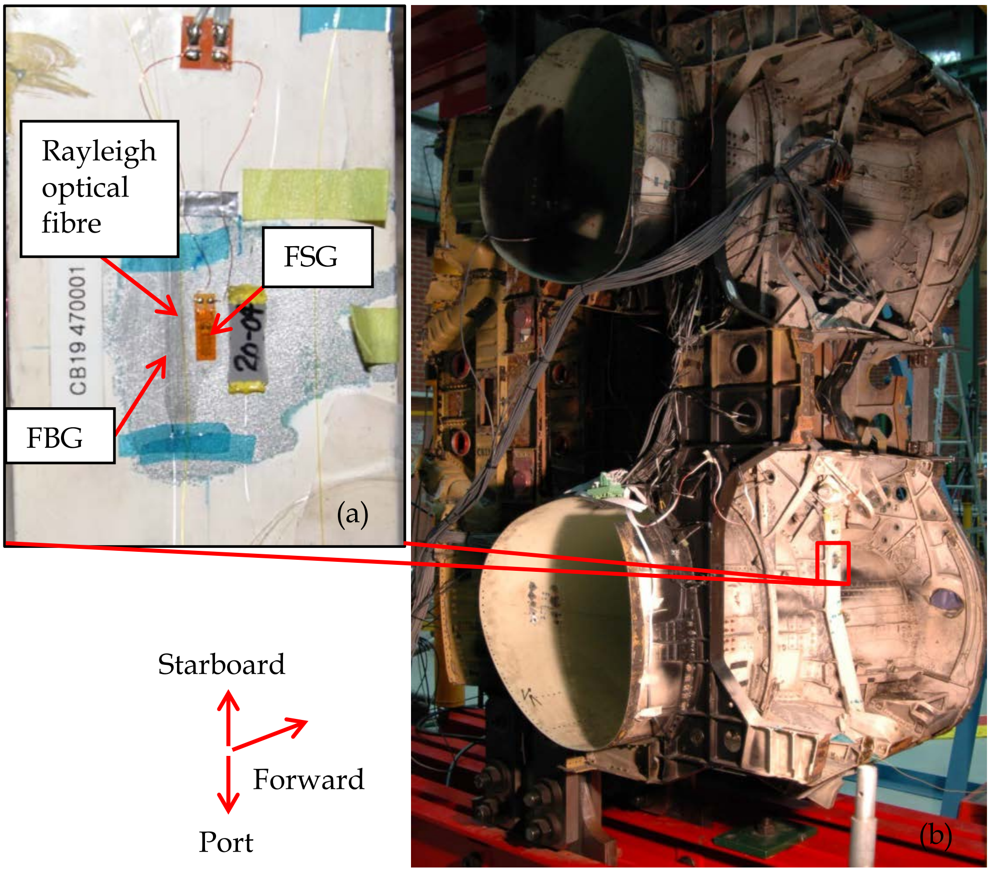


*Figure 20: (a) Close-up of strain sensors on the lower flange of the portside centre bulkhead; (b) Image of CB19 under test*

The measurements from the Rayleigh optical fibre were recorded in high and standard resolution modes using the ODiSI B. The measurements from the FBG were made using a Micron Optics si-425 optical interrogator and the FSG measurements were recorded using the existing data acquisition system for the Centre Barrel test program which was a Hewlett Packard (HP) 3852A data acquisition unit.

The CB was subjected to a stepped load survey in 10% increments up to 100% of the maximum spectrum load followed by a block of variable amplitude accelerated fatigue spectrum loading. Each block was applied twice so the Rayleigh system could acquire data in both high and low resolution mode.

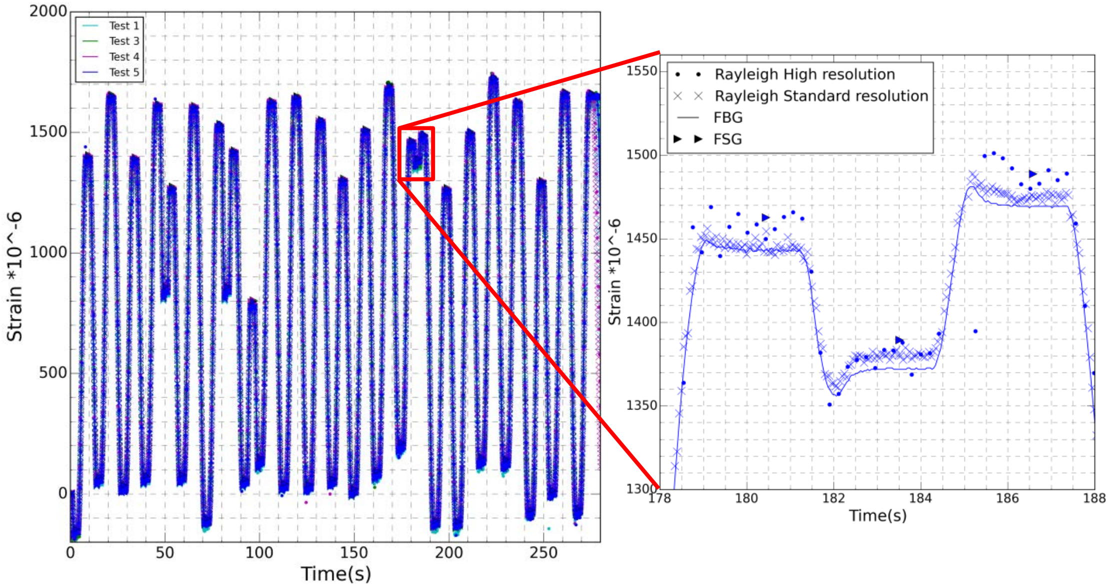


*Figure 21: Response of all sensors to spectrum loading; Inset: Strain response from test 5 over a 10 second interval.*

Figure 21 shows the measured strain response under spectrum loading at a single point as a function of time for the FSG, FBG and the ODiSi B system in high and low resolution modes. Strain measurements from four separate spectrum tests are overlayed in Figure 21 with the inset showing the strain response from a single test run (test 5) over a ten second measurement interval. The FSG measurement system was configured to only measure the strain at the turning points, thus only one point is recorded at each load cycle. The results show that there is reasonably good agreement between all measurement systems. The high resolution measurement showed a peak to peak noise level of 15 με (0.87% of peak strain) and the low resolution gave a peak to peak noise level of 10 με (0.58% of peak strain).The results from the FBG gauge by comparison show a much lower noise level.

Figure 22 shows the response of all the strain sensors at a single point during the 100% load survey. All five tests are overlayed with the insert showing a single test (test 1). The results show that there is reasonable agreement between all measurement systems. The high resolution strain measurement from the Rayleigh system over-estimates the strain by approximately 0.8% compared to the FBG measurement.

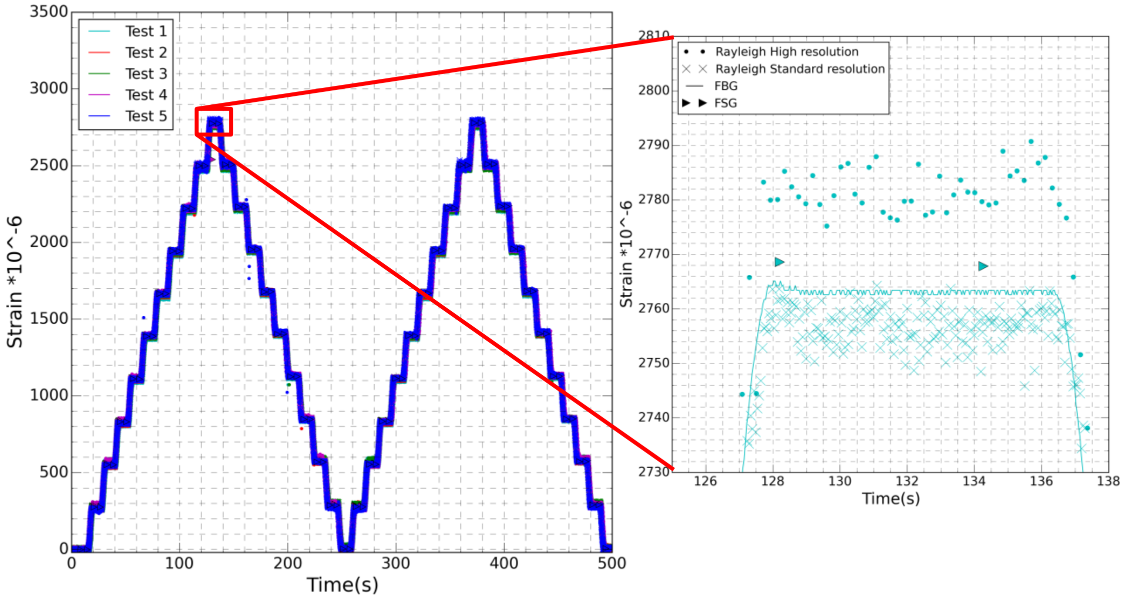


*Figure 22: Response of all sensors to stepped loading during 100% peak spectrum load survey; Inset: Strain response from test 1 over a 10 second interval.*

The noise level from the ODiSi B system is approximately 15 to 20 με for the high resolution mode and 10 to15 με for the low resolution mode which equates to 0.72% and 0.54% of the strain at this load level, respectively. The high resolution mode has a standard deviation in the signal of 5.4 με and the standard resolution mode has a 3 με standard deviation. As before the noise on the FBG measurement system is considerably less than the Rayleigh scattering measurement for both high and low resolution modes. Occasionally during this testing, some data drop outs and anomalous data points were observed from the ODiSi B measurements which correlated to momentary mechanical instabilities from the load actuation system during changes in the applied load.

## 5.3 Full Scale Fatigue Testing-Distributed Sensing

The final experiment investigated the potential of Rayleigh scattering to provide a broad area strain map from a dense optical fibre lay-up geometry. The strain distribution as measured by the optical fibre was compared to a full field stress map in the same region as measured by TSA. Unfortunately, there was no detailed FEA available in this region to enable a comparison with model predictions.

The measurement region was on the lower flange of the portside centre bulkhead (Y470.5) as shown in highlighted region of Figure 23 (a). The surface of the bulkhead in the measurement region was stripped of paint and protective coatings to expose the bare aluminium surface using Turco 5351. As the optical fibre and associated adhesive can interfere with the heat diffusion process, the TSA measurements were conducted first. The region of interest was spray painted with acrylic matt black paint to facilitate the TSA measurement. The CB was loaded sinusoidally to 8% of peak spectrum strain at 1 Hz for 20 to 30 minutes to acquire the TSA scan.

Afterwards the black paint was removed with acetone and the surface was cleaned and lightly abraded before adhering the optical fibre. A 10 m long fibre was laid up in parallel lines approximately 6.4 mm (±0.2 mm) apart along a flange length of 240 mm starting at the aft edge as shown in the inset of Figure 23. The fibre was bonded to the surface using the same adhesive as for the coupon testing (Norland Optical Adhesive, NOA-61). In this case, the adhesive was applied to the test area while it was in a nearly vertical orientation. To prevent the uncured adhesive running down the part, the adhesive was built-up in a series of light coats using a broad area Maxima ML-3500 S UV-A lamp to partially cure (30-60 secs exposure) the adhesive between coats. Three coats were applied to the fibre to cover the top surface of the fibre. After all the layers were applied, the region was fully cured under the UV lamp for 3 hours. The application of the fibre in this region required two operators, one to roll-out the fibre from the spool and pre-tension the fibre section and one to apply and cure the adhesive.

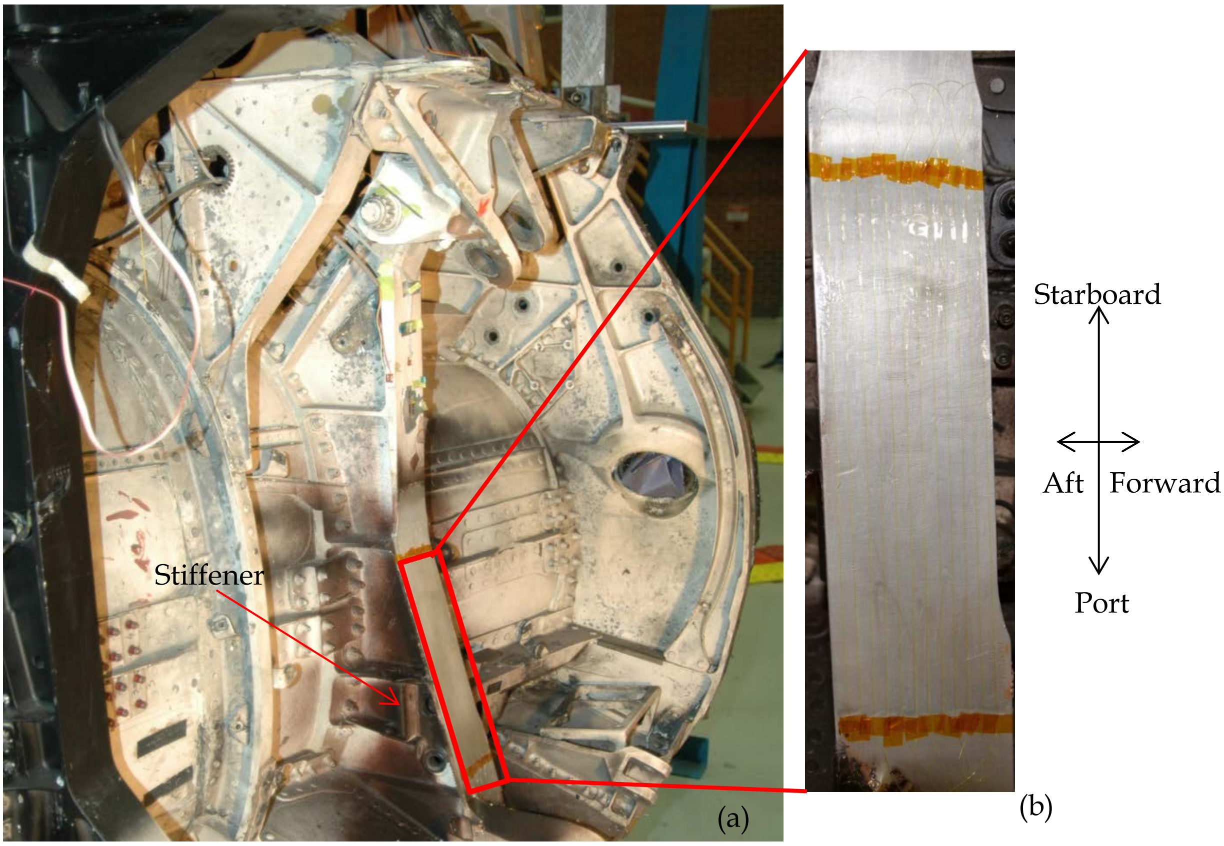


*Figure 23: Location of measurement area on the port lower flange of CB 19 centre bulkhead Y470.5; Inset: Close-up of the region showing the optical fibre lay-up geometry.*

Figures 24 (a) and (b) show the strain distribution in the lower bulkhead region as measured by the optical fibre in high and low resolution modes respectively. Figure 24 (c) shows the stress distribution as measured by the TSA. While a direct numerical comparison is not possible, the colour maps should show a similar distribution pattern as the stress and strain are directly proportional to one another. These colour maps show the entire region in compression with the dark blue representing the highest compression and the red the lowest compression.

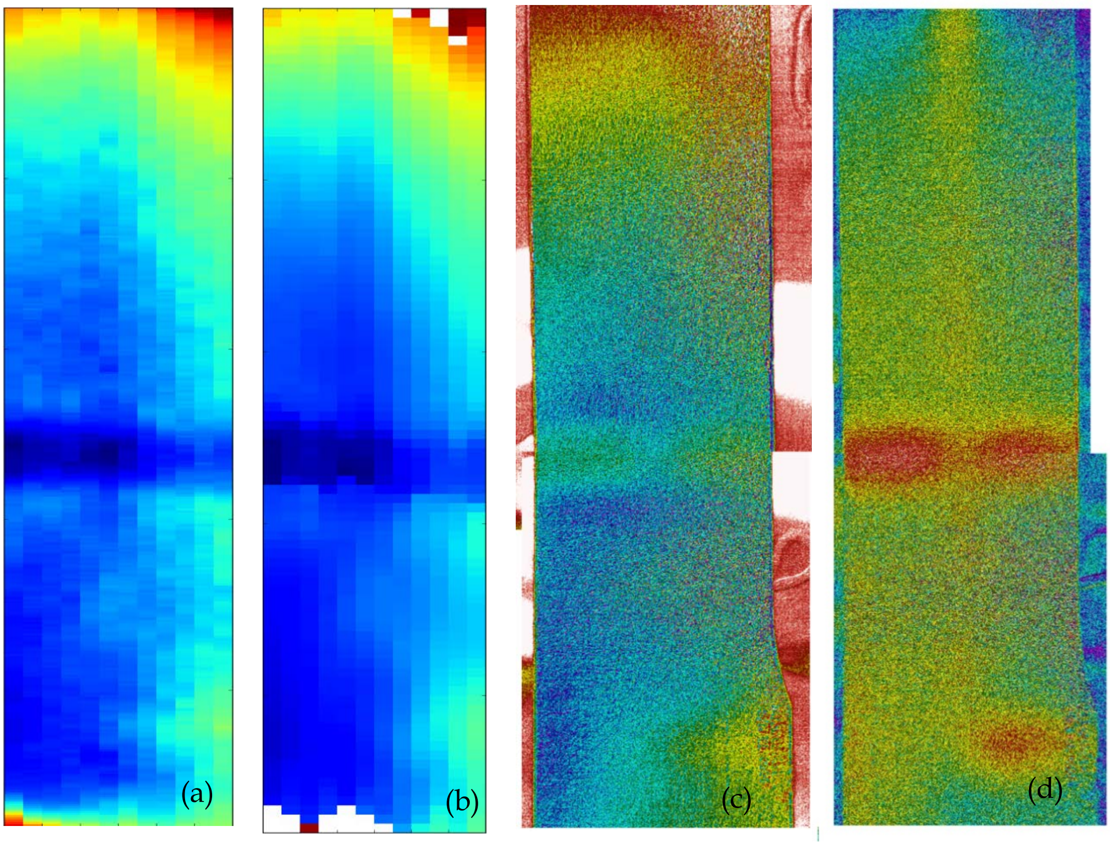


*Figure 24: Strain distribution across the port lower flange of CB 19 centre bulkhead Y470.5as measured by the optical fibres in (a) High resolution mode at 50% load; (b) Standard resolution mode 50% load. TSA scans showing (c) stress distribution and (d) quadrature at 8% load.*

The digitisation of the colour maps generated from the optical fibre measurements is a feature of the measurement spatial resolution. Although the strain distribution is broadly in agreement between the high and standard measurement modes, there is more noise observed in Figure 24 (a) as opposed to Figure 24 (b) where the strain contours appear less pixelated. In the standard resolution mode there are data drop-outs where the fibre transitions from a bonded to an unbonded region. This transition results in a large strain gradient from the region of the fibre which is experiencing the strain of the structure to the unconstrained fibre. These drop-outs were not observed in the high resolution measurement mode where the measurement has been shown to be more tolerant of strain gradients. Another notable feature of the colour maps generated from the optical fibre is the band of high compression in the centre of the measurement region. This coincides with an integral vertical stiffener located on the opposite side of the flange which appears to be acting as a stress concentrator when the flange is under compression. There is also a region in the bottom RHS of the flange which shows a localised drop in strain in the region where the flange increases in cross-section. There is also a vertical stiffener on the underside which could also be reducing the strains.

The stress distribution measured by the TSA is broadly in agreement with the strain distribution measured by the optical fibre. The most notable difference is that there is a reduction rather than an increase in compressive stress in the centre band of the flange. In order to investigate this further, the quadrature response from the TSA scan was recorded and is shown in Figure 24 (d). Ideally, the quadrature response across the structure should be uniform indicating an adiabatic response. However, in this case, there is non-uniform response along the flange and in the bottom RHS of the flange where the cross sectional area increases. This result shows that there is heat dissipation occurring in the structure because of the high strain gradients combined with a loading rate that is insufficiently high to ensure an adiabatic response. Unfortunately, it was not possible to increasing the loading frequency due to mechanical limitations with the load actuators. This means that stress measurements provided by the TSA scan will be erroneous in these regions. This result serves to highlight one of the potential drawbacks of full-field stress mapping using TSA, where it is not always possible to achieve an adiabatic response on complex structures under full-scale fatigue loading.

# 6. Spatial Offset Between Resolution Modes

Throughout all the experiments conducted as part of the testing of the ODiSI B there was a consistent spatial shift observed in the high resolution measurement with respect to the standard resolution measurement. The shift was estimated from the experimental measurements to be between 6.5 and 7.8 mm ahead of the standard resolution measurement.

Following communication with the manufacturer (Luna technologies) they confirmed that there is a spatial shift between the two measurement modes. The disparity between the modes is due to the fact that the coordinate system is mode-dependent. The following formula determines the difference:

Spatial Shift = (2 x standard resolution gauge length) – (2 x high resolution gauge length)

Using the specified gauge lengths of 5.12 mm and 1.28 mm for standard and high resolution mode gives a spatial offset of 7.68 mm which is within the range of the experimentally measured offset. The spatial shift is independent of the fibre length or geometry and may be corrected in the post-processing. Without this correction the location of features on the strain distribution map will not be accurate without a mode specific reference point.

# 7. Discussion

The ODiSI B distributed fibre optic strain measurement system has a measurement resolution and acquisition rate which are suitable for application to full-scale fatigue testing for broad-area strain distribution measurements. However, the measurement length and spatial resolution come at the cost of acquisition speed. In many cases, it is necessary to post-process the data to achieve the acquisition rates specified by the manufacturer. This results in very large data files that are time-consuming and processor intensive to process for long-term testing.

The experiments presented in this report show that Rayleigh scattering can provide distributed measurements of strain with reasonable agreement to point strain measurements made using FSGs and FBGs in regions where there is no significant strain gradient. The unfiltered noise levels on the strain measured by the Rayleigh system in the standard resolution mode are higher than FBG strain measurements and of a similar order to FSGs. In addition, the noise levels from the Rayleigh measurement system are higher when interrogating across a smaller spatial measurement interval (i.e. in the high resolution mode).

In regions of high strain gradient, the cross correlation software, which measures the shift in Rayleigh scatter between the strained and unstrained states, can fail to measure the shift reliably resulting in loss of data. In the experiments presented in this report, the level of strain gradient that the system could tolerate was between 100 and 150 με across a gauge length of 5.12 mm. In high resolution mode, strain gradients of up to 500 με across a gauge length of 1.25 mm were recorded before a loss of data occurred. For strain gradients approaching these levels, the strain measurement from the Rayleigh measurement underestimated the strain level by up to 10%.

The reasonably narrow lateral footprint of the sensing fibre (250 μm) means that relatively large distances between consecutive sensing lines are likely in many applications. For structural features or defects that cause highly localised strain perturbations, it is possible that the distributed fibre will not pick them up if they occur between the fibre optic sensing lines. Thus, distributed fibre optic sensor networks are unlikely to eliminate the need for full-field stress mapping techniques such as TSA. They do however, offer certain advantages over TSA in that there is no requirement to cyclically load the structure and the measurement region can be larger and in-situ for the duration of the test, allowing for damage initiation detection and tracking. Further work is required to compare the measured strain distributions on complex geometries to model predictions and asses their effectiveness in model validation and refinement.

The application time to bond a 10 metre sensing fibre to the FSFT was approximately 2 hours. Twelve sections of the fibre were bonded which provided approximately 5000 sensing points in high resolution mode, which equates to a cost of approximately 5 cents per sensing point (not including installation costs). There are further economies of scale with longer fibres and/or bonded areas. These represent significant cost savings over conventional FSGs, as well as savings in installation time. However, it should be noted that in order to ensure reliable strain transfer between the structure and the fibre, the fibre must be pre-tensioned and in close contact with the structure along the entire bonded length. Tight bend radii should be avoided to minimise optical losses and excessive stress on the fibre. There are engineering challenges in achieving this with a long fibre on a complex geometry. In addition, the aligning the sensing axis in the line of the fibre needs to be undertaken carefully. If the requirement is for a large number of multi-axial strain sensors (similar to FSG rosettes) at disparate locations across a large structure then the potential benefits of an all-optical distributed strain sensing system may be reduced.

# 8. Conclusion

In summary, the results from this preliminary testing have shown that the use of Rayleigh scattering from optical fibres to make distributed strain measurements shows promise for application to FSFTs. The benefits are greatest when the structure under test has a smooth flat surface profile and high density or high sensor count distributed measurements over a large area are required. Further testing will be required to develop and refine fibre lay-up and bonding processes for complex geometries, tri-axial sensing and to investigate the reliability and durability of the fibre, adhesives and the measurement under long-duration structural testing.

# References

[1] L. Molent, "A brief history of structural fatigue testing at Fishermans Bend Australia," *Advanced Materials Research*, vol. 891-892, 2014, 11th International Fatigue Congress, 104663, (2014).

[2] L. Molent, S.A. Barter, A comparison of crack growth behaviour in several full-scale airframe fatigue tests, *International Journal of Fatigue*, **29**(6), pp 1090-1099 (2007).

[3] Finney, J.M., Niessen, C., Absolom, N. and Lemm, K., "Strength and fatigue life enhancements of cracked metal" *DSTO-TR-0434* (1996).

[4] "Strain gauge Technology", Eds. A.L. Windoe and G.S. Holister. *Applied Science publishers* ISBN 0-85334-118-4, (1982).

[5] D. Samiec "Distributed fibre-optics temperature and strain measurement with extremely high spatial resolution," *Photonik international*, pp. 10-13 (2012).

[6] Kersey, A.D., Davis, M.A., Patrick, H.J., LeBlanc, M., Koo, K.P., Askins, C.G., Putnam, M.A., Friebele, E.J. "Fiber grating sensors" *Journal of Lightwave Technology*, 15 (8), pp. 1442-1462 (1997).

[7] Rao, Y.-J. "Recent progress in fiber-optic extrinsic Fabry-Perot interferometric sensors" *Optical Fiber Technology*, 12 (3), pp. 227-237 (2006).

[8] X. Bao and L. Chen, "Recent progress in distributed fibre optic sensors," *Sensor*s, vol. 12, pp. 8601-8639 (2012).

[9] Micro Measurements Instruction Bulletin B-127-14 ( Document No. 11127). Strain Gage Installations with M-Bond 200 Adhesive. Revision 29 June 2010.

[10] Van Roosbroeck, J., Jacobs, E., Voet, E., Vlekken, J. "Installation and test procedures of optical strain gauges for aeronautical applications." *Proceedings of SPIE* - The International Society for Optical Engineering, 7503 (2009)

[11] L. Molent. "The DSTO Contribution to the Fatigue Life Reassessment of the RAAF F/ A-18 Hornet Centre Barrel Structure." DSTO-TR-3062. (2015)

# Appendix A: ODiSI-B Measurement options

| PARAMETER | SPECIFICATION | | | | UNITS |
|---|---|---|---|---|---|
| **Performance** | | | | | |
| Standoff | 50 | | | | meters |
| Wavelength Accuracy[1,2] | 1.5 | | | | pm |
| Strain Range | ± 10 000 | | | | µStrain |
| Temperature Range[3] | -50 to 300 | | | | °C |
| **Mode of Operation[4]** | **Standard** | **High-Speed** | **High-Resolution** | **Extended Length** | |
| Maximum Sensing Length | 10 | 2 | 10 | 20 | meters |
| Acquisition Rate | 100 | 250 | 23.8 | 50 | Hz |
| Sensor Spacing | 2.56 | 2.56 | 0.64 | 2.56 | mm |
| Gage Length | 5.12 | 5.12 | 1.28 | 5.12 | mm |
| Strain Repeatability (Single-scan) | ± 5 | ± 5 | ± 20 | ± 10 | µStrain |
| Temperature Repeatability (Single-scan) | ± 0.4 | ± 0.4 | ± 1.6 | ± 0.8 | °C |
| **Electrical Trigger** | | | | | |
| Acquisition | TTL compatible | | | | |
| Event | TTL compatible | | | | |
| **Physical** | | | | | |
| Dimensions | 14 x 12.5 x 6.75 | | | | in |
| Weight | 17.3 | | | | lb |
| Power Consumption | 50 | | | | W |

1 Calibration is performed internally using a NIST-traceable HCN gas cell

2 Temperature and strain accuracies from spectral shift of Rayleigh scatter are 0.15 °C and 1.25 µStrain, calculated using the default conversion coefficients 1 GHz = 0.8 °C = 6.58 µStrain [Othonos and K Kalli, Fiber Bragg Gratings (Artech House, Boston, 1999)].

3 Based on material properties of the standard sensor: polyimide-coated, low-bend-loss optical fiber. For temperatures outside of this range, please contact your Luna representative for more information.

4 Base configuration includes one mode of operation. Additional modes are upgrade options.

| DEFENCE SCIENCE AND TECHNOLOGY GROUP<br>DOCUMENT CONTROL DATA | | | 1. DLM/CAVEAT (OF DOCUMENT) |
|---|---|---|---|
| 2. TITLE<br><br>Evaluation of a Distributed Fibre Optic Strain Sensing System for Full- Scale Fatigue Testing | | | 3. SECURITY CLASSIFICATION (FOR UNCLASSIFIED LIMITED RELEASE USE (U/L) NEXT TO DOCUMENT CLASSIFICATION)<br><br>Document (U)<br>Title (U)<br>Abstract (U) |
| 4. AUTHOR(S)<br><br>Claire Davis, Meg Knowles and Geoff Swanton | | | 5. CORPORATE AUTHOR<br><br>Defence Science and Technology Group<br>506 Lorimer Street<br>Fishermans Bend, VIC, 3207 |
| 6a. DST GROUP NUMBER<br><br>DST-Group-TR-3452 | 6b. AR NUMBER<br><br>AR-017-091 | 6c. TYPE OF REPORT<br><br>Technical Report | 7. DOCUMENT DATE<br><br>March 2018 |
| 8. OBJECTIVE ID | 9.TASK NUMBER<br><br>07/445 | | 10.TASK SPONSOR<br><br>Wing Commander Ravinder Singh (Deputy Director ASI) |
| 11. MSTC<br><br>Aircraft Health and Sustainment | | | 12. STC<br><br>Airframe Diagnostic Systems |
| 13. DOWNGRADING/DELIMITING INSTRUCTIONS | | | 14. RELEASE AUTHORITY<br><br>Chief, Aerospace Division |

15. SECONDARY RELEASE STATEMENT OF THIS DOCUMENT

*Approved for public release.*

OVERSEAS ENQUIRIES OUTSIDE STATED LIMITATIONS SHOULD BE REFERRED THROUGH DOCUMENT EXCHANGE, PO BOX 1500, EDINBURGH, SA 5111

16. DELIBERATE ANNOUNCEMENT

No limitations

17. CITATION IN OTHER DOCUMENTS

Yes

18. RESEARCH LIBRARY THESAURUS

Fibre optics, Rayleigh scattering, Structural health monitoring

19. ABSTRACT

This report details an experimental comparison between the performance of conventional electrical resistance foil strain gauges and a commercially available fibre optic distributed strain measurement system based on Rayleigh scattering. Results are presented which compare strain response, spatial resolution and noise levels between the two systems, firstly on coupon specimens containing fatigue-induced cracks and secondly on a full-scale fatigue test article consisting of a centre barrel of an ex-service F/A-18 under simulated operational loading spectrum.